Published in final edited form as:
J Appl Physiol (1985). 1991 June ; 70(6): 2351–2367.

Applications of fractal analysis to physiology

Robb W. Glenny, **H. Thomas Robertson**, **Stanley Yamashiro**, and **James B. Bassingthwaighte**
Department of Medicine and Center for Bioengineering, University of Washington, Seattle, Washington 98195

Abstract

This review describes approaches to the analysis of fractal properties of physiological observations. Fractals are useful to describe the natural irregularity of physiological systems because their irregularity is not truly random and can be demonstrated to have spatial or temporal correlation. The concepts of fractal analysis are introduced from intuitive, visual, and mathematical perspectives. The regional heterogeneities of pulmonary and myocardial flows are discussed as applications of spatial fractal analysis, and methods for estimating a fractal dimension from physiological data are presented. Although the methods used for fractal analyses of physiological data are still under development and will require additional validation, they appear to have great potential for the study of physiology at scales of resolution ranging from the microcirculation to the intact organism.

Keywords

mathematical analysis; heterogeneity; spatial correlation; temporal correlation; microcirculation; morphology; blood flow distribution

---

The Intent of this Review is to provide physiologists with the basic tools for working with fractals, by use of intuitive, visual, and formal mathematical definitions of the concepts of fractal geometry, self-similarity, scale independence, and fractal dimensions. Although the concepts underlying fractals are new, mathematical sophistication is not a prerequisite for a working knowledge of fractal applications. Applications of fractal analysis in physiology will be reviewed with examples from pulmonary morphology, pulmonary and cardiovascular circulation, and time-dependent analysis of physiological measurements. APPENDICES A and B include a glossary of terms and variables, a listing of the equations, and an illustrative analysis of a simple data set.

Fractal analysis is still in the formative stages of development, and its ultimate importance as an investigative tool in physiology is not fully established. Nevertheless, it is providing new perspectives into the physiology of cells, organs, and intact organisms, with mathematical models of branching structures and with descriptors of spatial and temporal correlation. The robust descriptive properties of this approach in the analysis of

---

Address for reprint requests: J. B. Bassingthwaighte, University of Washington, WD-12, Seattle, WA 98195.

physiological variability suggest that it may signal the development of a new paradigm (16) compelling the attention of investigators from diverse areas of physiological inquiry.

Self-Similarity and Fractal Dimensions

A fractal structure or fractal process can be loosely defined as having a characteristic form that remains constant over a magnitude of scales. A structure is fractal if its small-scale form appears similar to its large-scale form. Similarly, a process is fractal if a variable as a function of time undergoes characteristic changes that are similar regardless of the time interval over which the observations are made. In the parlance of fractal analysis, this is the quality of self-similarity, also termed scale independence. Because fractal analysis is not a familiar tool to most physiological investigators, we will systematically develop these principal definitions and concepts. Concurrently we will derive numerical methods to determine whether a structure or process is fractal and to estimate a fractal dimension.

The Koch curve (Fig. 1), created by the Swedish mathematician Helge von Koch in 1904, is a fractal structure that provides a simple introduction to the concepts of self-similarity and fractal dimensions. This curve is defined by the following iterative transformations. Beginning with a straight line of length l_0 (Fig. 1, top line), the middle third of the line is replaced with two segments of length 1/3 l_0, forming part of an equilateral triangle (Fig. 1, second line). The next iteration repeats the same procedure on each of the four resultant straight-line segments. Subsequent generations are formed in an identical fashion, and the completed figure represents the infinite expression of this iterative procedure. The completed Koch curve exemplifies the properties of self-similarity because, regardless of the scale used to examine any portion of the Koch curve, it maintains its characteristic form.

Examples of self-similar structures abound in the natural world. A tree maintains a quality of self-similarity independent of the perspective or scale from which it is viewed. The branching angles and proportionate diameters of branches appear to remain constant regardless of whether we are looking at the main trunk or the terminal branches. Clouds are fractal, with each billowing appendage similar in form to its entirety. In fact, without a reference scale, it is not possible to estimate the size of a cloud from a photograph (4). The classic example of fractal structures is a coastline, which appears to maintain the same degree of irregularity regardless of the size or detail of the map studied (23).

The bronchial tree can be visualized as a fractal structure, the final form of which is generated by an iterative process akin to that described above for the Koch curve (8, 24, 28, 42). The primordial lung bud initially undergoes a bifurcation to form the right and left bronchi, and subsequent generations are formed by a repetitive bifurcation of the most distal airways (18). In this manner, a dichotomously branching network is produced, filling the available space. In his initial description of potential fractal structures in nature, Mandelbrot (24) described a simple rectangular branching algorithm that bore a striking resemblance to the bronchial tree (Fig. 2, *left*). Since that first model, more realistic two-dimensional iterative transformation algorithms have been implemented on computers to simulate the growth and geometry of the bronchial tree (29). All these models exhibit the necessary

quality of self-similarity to be deemed fractal, in that each generation appears similar to previous generations, regardless of the level of bifurcation examined.

Contour-measuring method

A second principle of fractal structures and processes is a corollary of self-similarity: because the underlying form of a structure or process remains similar through successive magnifications of scale, it follows that a measured length of its form cannot approach a limit. Remembering the Koch curve, we can expand indefinitely the set of segments that contributes to its length. Although this property is a necessary requirement for a structure or process to be fractal in a strict mathematical sense, it is possible to discuss fractal properties of natural objects over a limited range of scales.

The Koch curve (Fig. 3, *left*) is a good model to formally examine the characteristic of the scale-dependent length of fractal structures. Because of its jaggedness, the apparent length [$L(l)$] of the curve will be dependent on the length (l) of the measuring device chosen. If we use a stick of length l_0, equal to the straight-line distance from one end to the other of the curve, none of the protruding structures will be measured and the apparent length of the entire line is l_0. If the measuring stick length l is decreased to 1/3 l_0 and then 1/9 l_0, the apparent contour length increases to 4/3 l_0 and 16/9 l_0, respectively. Generalizing this process for n iterations and a measuring stick of length $l = (1/3)^n l_0$, the corresponding measured length would be $(4/3)^n l_0$. Therefore, as l becomes infinitely small, or as $n \rightarrow \infty$, the apparent contour length of the Koch curve becomes infinite. As increasing magnification reveals more detail, the overall appearance of the new segment examined remains similar to that of the previous segment.

Mandelbrot (23) derived an "exponent of similarity," which he later renamed the fractal dimension (D), to characterize the complexity of fractal figures. D can be related to the Euclidean dimension (E). A line segment of E = 1 can be cut into N identical pieces. The ratio of the piece lengths (l) to l_0 is $l/l_0 = N^{-(1/1)}$. A square of E = 2 can be partitioned into N identical squares, and in an analogous fashion the ratio of the side lengths of the smaller squares to the initial square will be expressed by $l/l_0 = N^{-(1/2)}$. By the same process, a solid divided into N identical cubes will have side lengths that are scaled down from the original by a factor $l/l_0 = N^{-(1/3)}$. In each case, the ratio of the lengths is scaled down by $l/l_0 = N^{-(1/E)}$, where E represents the Euclidean dimension of the subdividing unit.

Similarly, a fractal figure will have a constant relationship between the number of pieces into which the figure is cut (N) and the ratio of the piece length to the total length measured at that particular choice of l, expressed again by

$$\frac{l}{l_0} = N^{-(1/D)} \quad (1)$$

where in this instance D is a fractal dimension (39). If N is expressed as $[L(l)/l]/[L(l_0)/l_0]$ in Eq. 1 and both sides of the equation are raised to the D power, Eq. 1 can be rewritten as $(l_0/l)^D = [L(l)/l]/[L(l_0)/l_0]$ or

$$\frac{L(l)}{L(l_0)} = \left(\frac{l}{l_0}\right)^{1-D} \quad (2)$$

For the Koch curve, in which $L(l)/L(l_0) = 4/3$ and $l/l_0 = 1/3$ for each iteration, D can be determined by substitution and solving the equation $1 - D = \ln(4/3)/\ln(1/3)$. The Koch curve therefore has a $D = \ln(4)/\ln(3) = 1.261$. … Unlike E, D is not usually an integer, but a fractal structure will always have a dimension equal to or less than the space in which the structure is defined (D < E).

Taking the logarithm of both sides of Eq. 2 and rearranging the terms yields

$$\ln L(l) = (1 - D)\ln\left(\frac{l}{l_0}\right) + \ln L(l_0) \quad (3)$$

In this form, a log-log plot of $L(l)$ vs. l/l_0 produces a line with a slope of (1 − D) and an intercept of ln $[L(l_0)]$. Figure 3, *right*, shows such a plot for the Koch curve, demonstrating a slope of −0.261 … or D = 1.261. … The value of the intercept is dependent on the arbitrary choice of l_0 and does not affect the determination of D. Equation 3 thus provides a working definition of a fractal process or structure. A process or object may be fractal if the logarithm of the measured value is linearly related to the logarithm of the scale of measurement. D is 1.0 minus the slope of this linear relationship.

An intuitive grasp of the meaning of a fractal dimension can be obtained from examination of some different fractal figures. A straight line has properties of self-similarity, in that at higher and higher resolutions it continues to show its same straight shape. It has a topological, fractal, and Euclidean dimension of 1. For different fractal line algorithms generated in two space, a topological dimension of 1 and a Euclidean dimension of 2 are maintained, but the more complex line figures have progressively increasing fractal dimensions. When the line becomes so complex that it nearly fills the plane, D_s approaches 2.0. Figure 4 illustrates some fractal curves that are iteratively produced by different rules, yielding different fractal dimensions (38). Even at the limited level of iteration illustrated in Fig. 4 the curves with higher fractal dimensions are more space filling. The fractal dimension therefore serves as a measure of complexity that is independent of the scale of magnification. As we will show later, this measurement of complexity can be used to characterize physiological structures and processes that have fractal properties.

Objects described by Euclidean geometry are not fractal. For example, a semicircle has no repeating characteristic form at different scales of inspection. Application of the contour-measuring method described for the Koch curve to the semicircle (Fig. 5, *left*) demonstrates that a semicircle is not fractal. For an initial measuring stick of l_0, if the distance around the semicircle is cut in half at each iteration (n), the apparent contour of the semicircle, $L(n)$, is dependent on n by the relationship

$$L(n)=l_0/[\prod_{i=1}^{n}\cos(\pi/2^{i+1})]$$

As $n \to \infty$, $L(n) \to \pi l_0/2$. Hence the semicircle is not fractal because its length approaches a limit as the scale of measurement decreases. Applying the log-log plot of contour length vs. measuring stick length (see Fig. 3) to the example of the semicircle shows that the slope of the plot rapidly approaches zero and therefore is not fractal (Fig. 5, *right*).

A measuring stick of length $(1/3)^n l_0$ was initially chosen to measure the Koch curve because it produces easily analyzed contour lengths. Another choice of measuring stick length would have been $(1/3)^{(n-1/2)} l_0$, which produces apparent contour lengths of $4^{(n-1/2)} l_0$ and D = 1.262. … A less optimal choice of measuring stick length yields a less accurate estimate of D. For example, measuring stick lengths of $(1/2)^n l_0$ and $(2/3)^n l_0$ produce estimated D of 1.216 … and 1.262 …, respectively. Figure 6 demonstrates the measurements on a Koch curve obtained from a stick length of $(2/3)^n l_0$, with the results plotted on a log-log plot as was done in Fig. 3. Note that, particularly at the larger stick lengths, more scatter is produced if only the first eight measurements of the apparent contour length are utilized. The least-squares estimate of D is accordingly incorrect, although it is apparent that this error will become less important if the measurements are continued with smaller measuring sticks. If finer measurements are made with smaller measuring stick lengths, the estimate of D will approach the theoretical D of 1.262. …

The accuracy of the measured contour length of a fractal line improves as the measuring stick gets smaller. The best estimate of D therefore should be determined from the measurements obtained using the smaller measurement segments, particularly in those circumstances where the optimal length of subdivision of the measuring stick is not known. Thus when working with experimental data, there is a rationale for excluding those measurements that were obtained using the largest measuring sticks and then fitting a least-squares regression line to the log-log plot of $L(l)$ vs. l/l_0. This approach ignores the information present in the larger measurements. Another approach is to fit a weighted least-squares linear regression to the entire data set. By weighting those measurements obtained using the smaller measuring sticks more heavily, a better estimate of D is obtained.

The confidence in an estimated value of D is dependent on the fit of the data to the regression line and the number of data points determining the line. Increasing the number of observations will improve the estimate of D by decreasing the variability in the measurement as the scale of measurement decreases. A statistical description of our confidence in the slope of the regression line can be determined from the standard deviation (SD) from the regression and arbitrary confidence intervals. The SD from the regression will actually be underestimated in these analyses because the observations are not independent of each other. When a measuring stick length of $(1/3)^n l_0$ is used to measure the Koch curve as in Fig. 3, *right*, we are certain that the slope of this line is −0.262 because of the perfect fit of the data to the line. However, we are only 95% confident that the slope of the line in Fig. 6 lies between −0.365 and −0.165 and that D is between 1.165 and 1.365. These issues

emphasize two important points about the experimental estimation of D. First, even for measurements on theoretically constructed fractal figures, the estimate of D is dependent on measurement sampling. Second, the confidence in the estimate of D can be strengthened by increasing the number of measurements obtained or using the optimal measuring stick, which decreases the variation of the measurements.

Finally in any real system, there will be measurement error, and this error will become more troublesome at the smaller measuring stick lengths. The effect of random noise superimposed on a fractal signal is to reduce the correlation. How this affects the estimate of D depends on the noise characteristics.

A relatively good linear fit between a variable and a measuring scale length on a log-log plot is not adequate proof that the variability of a process is explained only by its fractal properties. Such an observation does not exclude other nonfractal models, and it cannot establish whether a fractal model is better than any other. It is also important to recognize that a nonlinear relationship between two variables on a log-log plot does not prove that the relationship is not fractal. As shown in Fig. 6, a poor choice of measuring stick lengths or scale of measurements for a fractal structure may produce observations that do not appear linear. Rigaut (32) has proposed an alternative method for determining the D of log-log plots that are not linear. When the log-log plot is linear, Rigaut's method provides the same D as the least-squares regression method. However, if the line is curved, Rigaut's approach invokes a continuum of D values. The utility of his approach needs further exploration.

Box-counting method

Other methods for determining D use similar iterative scaling algorithms. A common method is the box or grid approach in which a fractal figure is covered with a grid or boxes of side length l (Fig. 7) and the number of boxes in which part of the figure is present is $N_{box}(l)$. By use of this technique, D can be determined from the slope of the log-log plot of $N_{box}(l)$ as a function of l. The advantage of this approach is that it can be efficiently coded as a computer algorithm and adapted to measure objects or processes in multiple (Euclidean) dimensions (20a). In practice, as was apparent with the measuring stick method, it is useful to examine as large a range of l as possible and to average D over a number of different placements of the grid or boxes (39). D is again usually determined from the slope of a log-log plot (L. S. Liebovitch and T. I. Toth, unpublished observations). The boxes do not have to be arranged on the rectangular grid but can be slid to minimize the number of boxes used at each level. This will merely shift the position of the line on the log-log plot and will not affect the estimate of D. Using this approach to determine D for the Koch curve in Fig. 7 yields an estimate of 1.23. Although close, this estimate differs from the theoretical value of 1.261 … because only a finite number of boxes and sizes can be used to measure a line that has infinite length.

A strict mathematical definition of a fractal structure has been offered by Mandelbrot (24) as a set for which the Hausdorff-Besicovitch dimension strictly exceeds the topological dimension. It is impossible to apply this definition to a set of physiological measurements where the mathematical structure of the variable of interest is not known. We have therefore chosen to define a structure or process as potentially fractal if it maintains a characteristic

form over many orders of magnitude of scale. A fractal structure or process can be tested for self-similarity by using the contour-measuring or box-counting method to determine whether there is a linear relationship obtained from Eq. 3. Although this definition cannot prove that a structure or process is fractal, it provides an estimate of D that can be used to characterize the irregularity or spatial and temporal correlation of a structure or process.

Although this approach using log-log plots provides an easily implemented means of testing whether a structure or process is fractal, uncertainties concerning the procedure remain. How sure are we that the structure or process is truly fractal as opposed to some other model such as an exponential decay process? There are not necessary and sufficient conditions to prove that the variability in real data sets is only fractal. A log-log linear relationship may be a necessary but insufficient requirement for some structures or processes to be characterized as fractal. Theoretical fractal structures have been described that have curved log-log plots, and the significance of this curvature and other nonlinear forms of these plots is not known. These issues are not resolved and will obviously be central to the future development of these approaches as a means of testing experimental hypotheses. Nevertheless, interesting preliminary results have been obtained in a number of physiological examples, as will be shown in subsequent sections.

Fractal Structures, Spatial Heterogeneity, and Spatial Correlation

Fractal analysis of morphology

Tree structures display self-similar characteristics, with their small-scale structures branching in a manner similar to their large-scale form. The mammalian bronchial and pulmonary vascular trees are richly arborizing structures that, despite their complexity, have a simple underlying order that spans many orders of magnitude in scale. A number of investigators have attempted to characterize this complexity and order in mathematical models with limited success. The self-similar nature of the bronchial and vascular trees suggests that fractal analysis may afford better mathematical models and provide some insight into their structure and morphogenesis.

Weibel and Gomez (41) used a simple exponential model to describe a unifying scaling relationship between the change in airway dimension and branch order. They collected morphometric data from casts of human lungs and found that an exponential relationship fit their data well up to the 10th generation but deviated significantly thereafter. The data of Weibel and Gomez have been reanalyzed by West et al. (42) using fractal analysis to show that their data can be better fit over the entire range of measurements by a fractal relationship between branch generation and branch diameter. Independent of scale or branch generation, the relationship of diameters between parent and daughter branches remains similar throughout all levels of the bronchial tree, demonstrating fractal properties of the airways. Fractal analysis in this particular example clearly provides a superior model in comparison to the original exponential model, inasmuch as the bronchial tree is more accurately represented over the entire range of the morphometric data.

Nelson and Manchester (29) have also used fractal analysis to explore the morphometric data obtained by others on the human airways. They used an approach similar to the

contour-measuring method in which their scale of measurement was the average branch length at a given level of the tree and the contour length was the total branch length of all segments for that level. Using data from Horsfield and Cumming (11) and Raabe et al. (31), they estimated D to be 2.64 and 2.76, respectively. In their analysis, the bronchial tree was modeled as a stick figure with no volume (topological dimension of 1) filling a three-dimensional space (E = 3). D = 2.64 and 2.76 therefore appear to be appropriate, inasmuch as these values lie between the topological and Euclidean dimensions.

Self-similarity has been recognized within the topology of the bronchial and pulmonary vascular trees for some time (9, 12, 22, 34). Using topological branching and ordering schemes developed for geographical stream analysis (Strahler ordering), Horsfield has shown that the ratio of mean diameters and lengths between parent and daughter branches remains relatively constant throughout all generations of the bronchial and pulmonary vascular trees. Excluding the 3 initial generations of 17 total generations in a human pulmonary vascular tree, the mean ratio of diameters between parent and daughter branches was 1.60 with a SD of only 0.056 (9).

With the advent of fractal analysis, Horsfield has reanalyzed his own data and confirmed that the bronchial tree is fractal; with the diameter and lengths of branches related to the branch generation by a log-log relationship (10). He compared fractal analysis of the bronchial tree with an exponential fit and concluded that the differences in the models are due primarily to the ordering system used to identify the branch generations. He also compared his analysis with West's and noted a difference in the linearity of their fractal models. West and associates (42) noted a sinusoidal variation in their data about a linear log-log relationship between the generation and the branch diameter and introduced a variable with a harmonic oscillation to improve the fit of their data. On the other hand, Horsfield found that his data nicely fit a linear relationship between the generation and the branch diameter. Horsfield (9) again ascribed this difference to the ordering system used to identify branch generations. The Strahler ordering system used by Horsfield is believed to be more correct for asymmetrically branching trees, and the fact that the fractal model provides a better fit to this ordering scheme may be evidence for this assertion (22).

Another interesting observation from Horsfield's data (9) and from Nelson's analysis of bronchial tree morphometric data (28) is that the first three generations of the trees do not conform to the fractal pattern of the rest of the lung. This suggests that the initial branchings of the pulmonary vasculature and bronchial tree are either not fractal or may have a different fractal dimension. Recent embryologic observations by Massoud and associates (26) have demonstrated that in fact there are two different branching patterns in the rat fetal lung, peripheral and central. The central branches of the pulmonary bronchial tree exhibit monopodial branching, while the rest of the tree divides dichotomously. This does not mean that the initial branches of the bronchial tree are not fractal, but rather they may follow a different fractal pattern of growth with a different fractal dimension.

Nelson and Manchester (29) have applied the concepts of fractal growth patterns to the embryologic development of the pulmonary vascular tree. They have developed two-dimensional models to study the effects of boundaries that limit the growth of the vascular

tree. They have shown that the development of the vascular tree can be modeled by fractal branching algorithms and boundaries that change as the embryo develops. These models develop strikingly realistic vascular patterns as shown in Fig. 2, *right*. With these models, simulations can be performed to study the effects of varying boundaries on developmental and morphologic structures (29). All these models are limited to two-dimensional space. More realistic models will have to branch into three dimensions. Although the computational effort will be greatly increased, the same fractal concepts that have been developed for two dimensions will be applicable to three dimensions.

Fractal structures are not confined to the pulmonary bronchial and vascular trees. Rigaut and associates (32) have used various magnifications and measuring lengths to estimate the boundary lengths of alveoli and found them to be fractal over a certain range. They also noted that their log-log plots of boundary lengths were not linear but tended to be convex upward. They interpreted this to show that the alveolar boundaries did not have a constant fractal dimension but rather what they termed a continuous fractal dimension transition (32). Fractal patterns have been used to characterize the complexity of neuronal cellular profiles (35). Smith and associates (35) used methods similar to the box-counting algorithm described above to characterize the contours of spinal cord neurons at different stages of maturity. They found that as the cells developed, they became more complex with D progressively increasing from 1.1 to 1.5. Sander (33) has shown that crystal growth patterns can be modeled and characterized by fractal analysis. In a process called diffusion-limited aggregation, a crystal starts as a seed point in the middle of a space. Particles are then introduced into the space and allowed to randomly move through the space until they touch the initial seed or a new part of the crystal. They stick to the crystal wherever they touch it and thus cause the crystal to grow. The structure of the resultant crystal can be characterized by fractal analysis. Other authors have used fractal growth patterns or diffusion-limited aggregation to describe the growth of the microvascular system (27, 36).

Fractal characterization of spatial heterogeneity using relative dispersion (RD) analysis

The observation that the vascular structures distributing flow to an organ are fractal suggests that the distribution of flow within the organ may be fractal as well. Although the small-scale variability in organ flow has been described as random, the branching structure of vascular anatomy suggests that regional flow is also best described by fractal measures. Heterogeneity of regional blood flow in an organ can be characterized by measuring the RD (SD/mean) of the regional flows when the organ is divided into a number of pieces. The observed RD is a sum of the spatial variation and the fluctuation of local flows over time (1, 3). When the distribution of flows is measured by a single rapid injection of a deposited flow marker, there is little contribution from the temporal fluctuations to the total heterogeneity.

When the heterogeneity of organ blood flow is characterized by this means, the calculated spatial RD (RD_s) is dependent on the size of the sampled pieces (1). If the blood flow in each of four pieces of an organ is measured, one can obtain the mean, SD, and hence RD of flow in the organ. If these same pieces are progressively subdivided, then for 8, 16, 32, 64, or more regions, the mean remains constant but the estimate of the SD and RD increases.

Even after appropriate corrections for experimental error, the largest estimate of RD_s will be obtained from the finest subdivisions of the organ (1).

The heterogeneity of organ blood flow can be characterized independently of scale by employing fractal analysis (1, 3, 5). The fractal equation describing the RD of flows for a given spatial resolution (piece size) is given by rephrasing Eq. 2, using RD_s as a function of a volume of size v

$$\frac{\mathrm{RD}_s(v)}{\mathrm{RD}_s(v_0)}=\left(\frac{v}{v_0}\right)^{1-D_s} \quad (4)$$

Here $RD_s(v)$ is the measured relative dispersion when the organ is partitioned into regions of volume v, $RD_s(v_0)$ is the RD_s found for an arbitrarily chosen piece size, and D_s is the derived spatial fractal dimension. Multiplying both sides of Eq. 4 by RD_s and taking the logarithms, we obtain

$$\ln\mathrm{RD}_s(v)=(1-D_s)\ln\left(\frac{v}{v_0}\right)+\ln\mathrm{RD}_s(v_0) \quad (5)$$

If the slope of log $RD_s(v)$ vs. log (v/v_0) is constant over a range of partitions, the system is said to behave fractally within that range. The greater the rate of increase in observable heterogeneity with an increase in resolution, the greater is the fractal dimension. The fractal dimension therefore serves as a measure of the scale-independent irregularity, roughness, or variation of a system (1). An advantage of this analytic approach is that it provides an estimate of D_s from easily obtained measurements of the RD_s of regional organ flow during successive subdivisions of the tissue pieces down to v_0.

Although regional blood flow to an organ is distributed in three-dimensional space, when characterized as a RD, the heterogeneity of flow is one dimensional (1, 3, 5). The limits of RD_s that are imposed by the analytic procedure can be explored by inspecting the two extremes of blood flow distribution: uniform flow and randomly distributed flow. In the instance of complete homogeneity, $RD_s(v) = 0$. Solving for D_s in Eq. 4 provides us with the lower boundary of 1.0 for D_s. For the case of random flow distribution, let there be distinct regions of flow that are distributed with a SD σ and mean μ. If the whole organ is partitioned into m pieces of volume $v_0 = v/m$, where v is the volume of the entire organ, the calculated $\mathrm{RD}_s(m)=\sqrt{\sigma^2}/\mu$. If the organ had been divided into n larger pieces of volume, $v = m/n \cdot v_0$, $\mathrm{RD}_s(n)=[\sqrt{(v_0/v)\cdot\sigma^2}]/\mu$, or $RD_s = (v/v_0)^{-1/2}(\sigma/\mu)$. Taking the logarithm of both sides yields the fractal form of the equation for a random flow distribution with a slope of −0.5 and thus a D_s of +1.5. In RD analysis a D_s of 1.0 indicates totally correlated magnitudes of flow between neighboring regions of the organ in that the flow is the same everywhere, while a D_s of +1.5 indicates that the magnitude of flow is uncorrelated or randomly distributed among neighboring pieces of the organ. D_s values ≥ 1.5 indicate inversely or negatively correlated flows.

Pulmonary blood flow distribution can be characterized by fractal methods (5). A composite fractal plot of the $RD_s(v)$ for six supine dogs is presented in Fig. 8. D_s for these animals ranged from 1.07 to 1.12 with an average of 1.09. The data fit the fractal model well, with an average correlation coefficient (r) of 0.98. It is interesting to note that the observed measures of RD_s appear to oscillate about the linear regression line. As discussed earlier, this may be due to the fact that the lung pieces (measuring stick) are not the proper shape or orientation for our measurement. The appropriate sectioning of the organ would be along the vascular tree, with regions of common perfusion being grouped together. The data points shown in Fig. 8 do not include the first four subdivisions of the lungs, because those measurements are disproportionately smaller.

The heterogeneity of myocardial blood flow has been characterized by fractal analysis as well (2, 3). The distribution of radiolabeled microspheres to the heart was analyzed by progressively subdividing the heart into finer pieces. In this original application of the RD approach, regional flows were normalized to mass rather than to volume. The spatial heterogeneity of cardiac blood flow in baboons, sheep, and rabbits, as characterized by the fractal dimension, is shown in Table 1, along with the fractal dimensions for pulmonary blood flow in dogs. Although the number of pieces in the cardiac data sets is relatively small, the fractal dimensions are significantly different between some of the species and organs. This indicates that the spatial distribution of flow is different among these organs and suggests that this is necessary for their different functions or is due to dissimilar morphogenesis.

This comparison demonstrates an advantage of fractal analysis in that comparisons of measurements can be made between experiments, species, and laboratories, regardless of units or scales of measure. The heterogeneity of blood flow in the hearts of baboons and sheep measured by one technique can be compared with the heterogeneity of blood flow in dog lungs measured in another laboratory by use of very different methods.

Blood flow heterogeneity can be fractal only over a limited range. If smaller and smaller pieces are used to measure flow to a region of tissue, eventually the flows will become more similar as the anatomic limit of a capillary is reached (1). As long as heterogeneity is fractal, the log of RD_s will remain linear with respect to the log of the volume of pieces. However, as the functional unit of perfusion is approached with smaller piece sizes, RD will stabilize, causing a plateau in the fractal plot (1). Theoretically, fractal analysis could identify the size of the functional unit of flow in a lung by finding the piece size where there is an inflection in the slope of the fractal plot (1). The method we used to measure regional blood flow distributions could be used to examine 24-mm^3 pieces of lung. No inflection point could be detected, suggesting that the unit of uniform perfusion is <24 mm^3. However, registration error between the true vascular boundaries and the imposed partitioning may cause the plateau to be slurred and produce an underestimate of the size of the unit of perfusion (5).

Fractal analysis of spatial correlation

The measurement of spatial blood flow heterogeneity implies a measure of correlation as well. The fractal dimensions of regional pulmonary and myocardial blood flow indicate that flow is not randomly distributed but rather has some spatial organization. The spatial

correlation of flow is a measure of the similarity of flow magnitudes between neighboring regions of the organ. This spatial correlation is apparent when the local blood flow distributions are examined in isogravitational lung slices (5), in that high-flow regions tend to be near areas of high flow and low-flow regions usually are adjacent to other low-flow areas. The RD method used to characterize the spatial heterogeneity of organ blood flow maintains spatial information by always aggregating nearest neighbors. Van Beek et al. (37) have shown that the spatial correlation of flows within an organ can be determined from D_s.

The relationship between the spatial correlation of blood flow and D_s can be ascertained by exploring the expected RD of flow to combined neighboring regions of an organ. If adjacent pieces, Y_1 and Y_2, are combined, the expected flow, $\overline{(Y_1+Y_2)}=2\mu$, and the variance of the aggregated regions, Var (Y_1 + Y_2) = Var (Y_1) + Var (Y_2) + 2 Cov (Y_1, Y_2), where Cov is the covariance. Because Var (Y_1) = Var (Y_2) = Var (Y) the RD of the combined pieces is

$$\mathrm{RD}_s(Y_1+Y_2)=\frac{1}{\sqrt{2}}\cdot\frac{\sqrt{\mathrm{Var}\,(Y)+\mathrm{Cov}\,(Y_1,Y_2)}}{\mu} \quad (6)$$

$\mathrm{RD}_s(Y_1 + Y_2)$ can also be defined by the fractal Eq. 4

$$\frac{\mathrm{RD}_s(Y_1+Y_2)}{\mathrm{RD}_s(Y)}=\left(\frac{Y_1+Y_2}{Y}\right)^{1-D_s}=2^{1-D_s} \quad (7)$$

If the correlation of flows between adjacent regions is the same correlation used for the linear regression of two variables, then the spatial correlation r_s = Cov (Y_1, Y_2)/Var (Y). Equations 6 and 7 can be rewritten in terms of r_s

$$r_s=2^{3-2D_s}-1 \quad (8)$$

where D_s is bounded by 1.0 and 1.5.

As predicted by Eq. 8, a uniform blood flow distribution to neighboring pieces of tissue (D_s = 1.0) is perfectly correlated with r_s = 1.0, while a random blood flow (D_s = 1.5) is completely uncorrelated with r_s = 0.0. When the D for baboon heart, sheep heart, and dog lung blood flows are substituted into this equation, regional r_s = 0.49, 0.58, and 0.76, respectively, (Table 1).

Equation 8 tells us that if blood flow distribution in an organ is fractal, then, regardless of the location of the region examined, blood flow to neighboring regions of tissue is also correlated. In Fig. 9, a schematic representation of regional vascular perfusion to an organ, the correlation of blood flow between pieces *AAA* and *AAB*, is the same as between pieces *ABA* and *ABB*. A second consequence of Eq. 8 is that if the blood flow distribution is fractal, blood flow to neighboring pieces of an organ is correlated regardless of the size of the pieces. This means that in Fig. 9 the correlation of blood flow between pieces *A* and *B* is the same as between *AA* and *BB* as well as between *AAA* and *AAB*.

A similar derivation of r_s can be done for pieces of tissue formed by aggregating more than two neighboring pieces. This is the extended-range correlation technique of Bassingthwaighte and Beyer (44), which is given as the last equation in the APPENDIX and can be applied to isotropic or anisotropic spatial intensities. The correlation between regions falls off with increasing separation between them. The rate of fall off of r_s is exactly the same for all sample sizes, a fractal "self-similarity," and asymptotically follows a power law with a log-log slope of $2.0(1 - D)$ for $1.0 \leq D \leq 1.5$. The fall off is less rapid than an exponential; i.e., the correlation extends over a longer range of separation.

Fractal modeling of vascular trees

Let us return to our original assertion that the regional distribution of organ blood flow may be fractal because the vascular structures distributing the flows are fractal themselves. We can test this hypothesis by modeling the pulmonary vasculature as a fractal structure and examining the distribution of flows produced by such a model.

A simple vascular model can be depicted by a main stem vessel with repetitively bifurcating daughter branches (Fig. 10). At each generation the number of branches doubles, producing 2^n terminal branches after n generations. If the diameters and lengths of daughter branches are recursively defined by the parent branch, the vascular structure will be fractal with respect to the diameters and lengths (37). If the relative fraction of flow distributed to each of the daughter branches remains constant throughout all generations, the fraction of flow to one daughter branch can be represented by γ and the fraction of flow to the other branch is therefore $1 - \gamma$. If the flow in the main stem vessel is F_0, the flow at any branch can be determined and the flows emerging after n generations have the values

$$F = \gamma^k (1 - \gamma)^{n-k} F_0 \quad (9)$$

where k assumes integer values from 0 to n. The flow distribution in this model is skewed to the right and is similar to that seen in hearts and lungs. If $\gamma = 0.5$, the branching is symmetrical and flows are uniform, while deviations of γ away from 0.5 produce heterogeneity. Fixed values of γ differing by 0.03 or 0.04 from 0.5 and random values for $\gamma = 0.5 \pm 0.04$ give good fits to organ flow data. All these values are slightly curved on log-log plots. As noted previously, the significance of this curvature is a theoretically fractal structure is not clear.

When the observed distributions of blood flow in an organ are modeled by this asymmetrically bifurcating network, a γ can be determined for the best fit to the actual RD data. The observed RD and the theoretical RD for the best-fitting γ are shown in Fig. 11 as a function of the piece size for a given dog lung. The mean coefficient of variation between this model and the experimental data was 0.070 ± 0.042 (6). The γ that best fit the RD data for baboon hearts, sheep hearts, and dog lungs are 0.461 ± 0.007, 0.451 ± 0.022, and 0.459 ± 0.009, respectively (37). It is evident that this simple fractal network accurately models the observed RD values over a large range of piece sizes.

The estimated branching asymmetry of this fractal network can be compared with the branching asymmetry of the human pulmonary vasculature quantitated by morphological techniques. Horsfield and Woldenberg (13) measured the diameters of parent and daughter branches at 1,937 bifurcations in casts of saline-filled fully inflated lungs. They determined that the mean ratio of daughter diameters was 1.274. Using Poiseuille's law, this would be equivalent to $\gamma = 0.365$. This degree of asymmetry would produce a flow distribution with RD = 136% after only 15 generations. This appears to be unreasonably large compared with the measured RD of ~35% in dog lungs after a similar number of generations (5). A possible explanation for this discrepancy is that the morphological measurements were made on saline-filled fully inflated lungs with casting resin injected at a pressure of 40 cmH_2O, while the measurement of flow distributions in the dogs was made on intact animals at functional residual capacity. The observation that the physiologically measured heterogeneity of flow is less than predicted by anatomic measurements may also suggest that, in intact animals, local regulatory mechanisms could limit the heterogeneity of blood flow.

The fractal branching model is not meant to be a precise representation of anatomic structures. Rather it emphasizes the concept of how small degrees of asymmetry in flow can produce heterogeneous blood flow distributions similar to those seen in experimental studies. The precise value of γ or σ is of little importance relative to this idea. The fractal branching model offers a possible mechanism to explain the observed heterogeneity of pulmonary blood flow within isogravitational planes. By use of the concepts of fractals, this model is able to relate the function and structure of the pulmonary vascular tree and offer an explanation for the spatial distribution and gravity-independent heterogeneity of blood flow.

Fractal Process, Temporal Heterogeneity, and Temporal Correlation

The concepts of self-similarity and fractal dimensions can also be applied to observations made over time. Examples of appropriate time-dependent variables abound in physiological studies, including fluctuating ionic currents, blood flows and pressures, and ventilatory excursions. Several methods of eliciting the underlying dimensionality of such measurements have been developed for time series data. These fall into two classes: *1*) dispersion analysis, which gives a measure of local correlation, and *2*) minimal order analysis, which defines the minimal order of a set of differential equations describing the chaotic dynamic behavior of the system that is fluctuating unpredictably while remaining bounded and self-correlated. Although each of these approaches defines fractal measures, described by a fractal dimension, they are quite different. Dispersion analysis reduces the complexity of the system, regarding it as one-dimensional, while the time series analysis for the dimension of a chaotic signal attempts to define the minimal degree of complexity or order of the system. Minimal order analysis is not discussed here.

Dispersion analysis

Three basic methods of dispersion analysis can be applied to temporal observations, one using the RD (RD_t), the second using Hurst's rescaled range, and the third being the measure of extended-range correlation. The simplest analysis is the application of RD described above for spatial variation (3). The application to a signal $V(t)$ is shown in Fig. 12,

where V(t) may be any measure such as voltage, velocity, or position. A digitized signal measured at uniform intervals (τ_0) can be considered as a population of observations in one dimension. $RD_\tau(\tau_0)$ is initially calculated for all the sampled data in the upper row of Fig. 12. Pairs of neighboring points are then averaged to obtain the second row, and $RD_\tau(2\tau_0)$ is calculated. Recursive pairing to double the interval length and recalculation of the SD on the combined data points gives $RD_\tau(4t_0)$, $RD_\tau(8t_0)$, … $RD_\tau(N\tau_0)$ for each row of "observations" in Fig. 12. When $RD_\tau(N\tau_0)$ and N are plotted on logarithmic scales, they are well characterized by a fractal relationship, which is a straight line

$$RD_\tau(N\tau_0)=RD_\tau(\tau_0)N^{1-D_\tau} \quad (10)$$

D_τ for this random signal is 1.5, so the exponent of N is −0.5. This result indicates that with each doubling of the averaging interval to $2t_0$, $4t_0$, etc., the RD_τ scales down by $1/\sqrt{2}$, i.e., to 0.707 of the RD_τ at the next smaller interval duration. As was the case with the measuring stick length for the contour length method, there is no particular need to use interval doubling, because any increment will give a similar D_τ, provided enough data points are available. The D_τ of 1.5 is that expected for any random signal. In this case, the random signal was Gaussian with a mean of 1.0 and an SD of 0.3. The r, given by Eq. 8, is zero in this case. The same D_τ would be found for other random signals, uniform over an interval such as Poisson or random walk. The information from this analysis is limited to the variance and does not characterize the form of the distribution or higher moments such as skewness and kurtosis.

Fractal analysis of time-dependent observations provides a means for characterizing temporal correlation in a fashion similar to that of spatial correlation. Correlation over time is also described as memory. If a fractal process with positive correlation is trending upward, adjacent observations in time will also tend to increase, and similarly if the process is trending downward, neighboring observations in time will likely be decreasing as well. In other words, the state or position of a process, V(t), is influenced by its previous values V(t − 1). Negative temporal correlation signifies that adjacent values in time tend to move away from each other.

When the RD_τ analysis was applied to the time series data on erythrocyte velocities from Kislyakov et al. (15), a D_τ of 1.37 was found. The more extensive data of Oude Vrielink et al. (30), shown in Fig. 13, *left*, allow a more accurate test for a fractal relationship. The RD_τ vs. τ relationship (Fig. 13, *right*) gives a D_τ of 1.16, indicating correlation with the coefficient r = 0.60. The fact that there is correlation is intriguing and invites further experimental work and other analyses to determine the basis of the correlation. It is important to emphasize that this similarity of adjacent observations over time holds true over the entire range of the time intervals examined. The statement that observations adjacent in time are similar is not the important conclusion of this analysis but, rather, that this is a fractal process in which the relationship between successive measurements is consistent on all time scales.

Hurst's (14) “rescaled range analysis” is similar to the RD analysis and can be applied to spatial as well as temporal data. In the simplest version of this method (4), the SD is normalized by dividing it into the local range (R) of the cumulative differences from the mean over the interval of length τ, rather than by the mean as in the RD analysis. R generally increases with the interval duration, but SD changes little. The approach is to plot the log R/SD vs. log τ. The slope is H − 1, where H is the Hurst coefficient

$$\frac{R/\mathrm{SD} \quad \text{for} \quad \text{interval}\,\tau}{R/\mathrm{SD} \quad \text{for} \quad \text{interval}\,\tau_0} = \left(\frac{\tau}{\tau_0}\right)^{H-1} \quad (11)$$

The R/SD grows with the interval length τ, as might be expected because the dispersion is in the denominator. The values of R/SD are very scattered for short τ or few observations, but the information content is very similar to that provided by the RD analysis, and H is related to D

$$H = 2 - D \quad (12)$$

The approach is good when H = 0.5 (random, no correlation) and when H > 0.5 (correlated functions with “memory”). The *r* between adjacent intervals is $2^{2H-1} - 1$, the same as in Eq. 8.

Both the RD analysis and rescaled range analysis need to be carefully evaluated by extensive testing. The RD analysis appears more robust, particularly for smaller data sets, and may be less subject to the skewing attendant on dividing by individual values of SD within each interval, as in the rescaled range analysis. Hurst's original method is more precise than described above or by Feder (4) in that it accounts for local trends in the data.

The extended-range correlation technique of Bassingthwaighte and Beyer (44) is a test of the fractal nature of a time series. The two-point autocorrelation is determined for units separated by *n* units, giving a statistical measure of *r*(*n*) for any *n*

$$r(n) = \frac{\sum x_i(\tau) x_i(\tau + n\tau)}{\mathrm{Var}\,(x)} \quad (13)$$

The theoretical fractal curve for the correlation is

$$r(n) = {}^{1}/_{2}\left[|n+1|^{2H} - 2n^{2H} + |n-1|^{2H}\right] \quad (14)$$

which for $n > 3$ follows a simple relationship that is a straight line on a log-log plot, $r(n)/[r(n-1)] = [n/(n-1)]^{2H-2}$. Thus H can be calculated directly from the slope, H = (slope + 2)/2.

These methods bear a relationship to Fourier analysis where one obtains the relative power and phase at each frequency. When the logarithm of the amplitude of the individual frequency components of the signal vs. the logarithm of the frequency is plotted for fractal signals, the slope of the relationship between the two components can be a straight line with

slope $-\beta$ (39). The fractal self-similarity demonstrated in this analysis is the constant ratio of power at any two frequencies, independent of the resolution (the position of the frequency scale). In this context, white random noise (all frequencies with equal power) has $\beta = 0$ and so-called Brownian noise has $\beta = 2$. Sets of noise with amplitude proportional to $f^{-\beta}$ exhibit memory. Over this limited range

$$\beta = 2H - 1 = 3 - 2D_\tau \quad (15)$$

Goldberger et al. (7) have used frequency analysis to characterize the fractal nature of the electrocardiographic signal. They argued that an electrical stimulus passed through a fractal network should result in a voltage-time pulse with a power spectral density that has a linear relationship on a log-log plot. They asserted that the His-Purkinje conduction network is a fractal structure and should therefore produce a fractal process. In testing this hypothesis, using a fast Fourier transformation, they examined a single QRS complex from 21 resting subjects. When they plotted the logarithm of the mean square of the amplitudes against the logarithm of the frequency for the mean data of 21 subjects, they found a power-law relationship.

Many natural signals including ionic channel noise (20), speech intensities (39), Nile River flood levels (14, 25), and rain (21) are analogous to correlated noise, with $0.5 < \beta < 1.5$. Most interestingly, music of almost all cultures (40) shows frequency and intensity changes with $\beta = 1$. These have been characterized by how the amplitude of V(t) varies between points in time, such that

$$\Delta V = k\Delta t^H \quad (16)$$

For H = 0.5, ΔV is typical Brownian motion, and for 0.5 < H < 1.0, there is positive correlation between neighboring points. Commonly, natural phenomena show H's of 0.7–0.8 (14).

Utility of Fractal Analysis, Structures, and Processes

One advantage of applying fractal analysis to biological systems relates to the analogy between the mathematical structure of fractals and the patterns of growth of the neural, vascular, and airway pathways. The evolution of multicellular organisms has mandated the development of connections between the environment and each individual cell. These branching connections must make the transition from large to small and simple to complex as efficiently as possible. An example is the transport of respiratory gases between the environment and alveoli along the dichotomous fractal branching of the airways, which transforms a simple 3-cm^2 tracheal cross section to a complex 70-m^2 alveolar surface area. The blood reaching the alveolar capillaries undergoes a similar transformation from a single large vessel to a complex capillary network by means of fractal branching. The fractal description of these network patterns is logical and based on the scale-independent similarity of these systems over several orders of magnitude.

With increasingly greater spatial and temporal resolution of physiological measurement, it is becoming evident that biologic systems are not smooth continuous processes. They do, however, maintain a degree of spatial and temporal correlation. Fractal analysis permits the characterization of these processes or structures that are not easily represented by the traditional analytic tools. By providing a geometric framework for the description of apparently irregular patterns, fractal analysis is able to characterize natural structures (36). Biological structures as diverse as protein surfaces, neuronal cell contours, and the bronchial tree can be succinctly characterized by fractal analysis (19, 35, 42). This unifying strategy allows characterization and comparison of a vast array of physiological systems.

The construction of self-similar structures reveals a potential advantage in coding for the growth and development of the necessarily complex vascular, neural, and airway networks. Complex mathematical fractal figures can be constructed from simple recursive algorithms (39). This recursive quality of the mathematical kernel permits a concise description of remarkably complex structures (43). Because there cannot possibly be a complete genetic description for the construction of every alveolus and capillary, it seems logical to propose that there are elementary recursive rules to guide their construction. These construction codes are probably not fractal themselves but are likely deterministic rules defining basic elements that are influenced by the environment in which the structure grows. The branching structures of the vascular system and the bronchial tree are such examples, where it is not known whether the branching angles and diameters are determined by the parent branch or by the similar environment in which they are constructed. Although the mechanisms by which these rules operate are speculative, a coding for self-similar structures is clearly the most efficient and appropriate algorithm to explain both the order and complexity of ontogeny. The efficiency of the finalized structures is also of importance to the organism. Lefèvre (18) has shown that a self-similar branching model of the pulmonary vascular system optimizes the cost-function (energy-materials) relationship while closely approximating physiological and morphometric data. Tsonis and Tsonis (36) have related fractal patterning to minimal energy consumption as well. If the development of biologic trees such as the bronchial and vascular systems can be modeled by fractal structures, then these models can also be used to investigate the effects of boundary limitation on these trees (29).

With these new analytic methods for characterizing physiological systems, physiologists are faced with a problem similar to that in the parable of the blind men attempting to describe an elephant. Although we can accurately describe single characteristics, we lack the perspective to determine the best approach for characterizing complete systems. Fractal analysis using the RD or frequency domains can be applied to any spatial or temporal physiological measurement. At present, we need to explore each of the different techniques to determine the relative advantages and limitations of each when applied to physiological systems. Our recommendations to those wishing to use these methods is to try them all, because each approach may provide unique information. From a practical standpoint, the limiting factor with these analytic methods is data set size. As a first approximation, at least a few hundred data points are required for the dispersional analysis and more would obviously improve the dimensional estimates obtained.

In this review we have focused on the various fractal measures of correlation in spatial properties and temporal fluctuations. Physiologists seek insight into biological mechanisms from the variable signals of life processes such as measurements of pressures, frequencies, and flows. The traditional analytic tools have been measures of means and variances with statistical approaches based on the assumption of random error in the measurements. The fractal revolution has brought the realization that this “error” can be analyzed as a fundamental property of the biological system that may include complex information with structure defined by these new analytic techniques.

Acknowledgments

This study was supported by National Heart, Lung, and Blood Institute Grants HL-08155, HL-38736, and RR-1243 and by Grant 89-WA-515 from the American Heart Association—Washington Affiliate.

Appendix A

Definitions

Box measurement	A method of estimating fractal dimension by covering the structure to be analyzed with boxes of various side lengths
Contour measurement	A method of estimating fractal dimension using measuring sticks of various lengths
Euclidean dimension	Integer representing the fewest coordinates required to represent an object in traditional Euclidean geometry. Euclidean dimension of a straight line is 1, that of a curved line or plane is 2, and that of a curved surface or sphere is 3
Fractal dimension	An estimate of the scale-independent complexity or irregularity of a system over space or time. It can assume all real values greater than or equal to the topological dimension and less than or equal to the Euclidean dimension
Fractal structure	An object that has a characteristic form that remains constant over a magnitude of scales, an object with small-scale structure similar to its large-scale structure
Fractal process	A variable as a function of time with fluctuations over a short time scale similar to those over a longer time scale
Heterogeneity	A measure of nonuniformity
Hurst exponent	A measure of complexity or irregularity of a system over space or time determined from rescaled range analysis. It can assume all real values between 0.5 and 1.0 and is related to the fractal dimension (D) by the equation $H = 2 - D$, where D is either D_s or D_τ
Koch curve	A self-similar geometric structure defined by a series of repeated transformations first described by Helge von Koch in 1904 (see Fig. 1)
Memory	Characteristic of a time-dependent variable that has temporal correlation. It signifies that a positively correlated process will tend to continue moving in the same direction. $V(t)$ is influenced by $V(t - 1)$
RD analysis	A method of estimating a fractal dimension using the measure of relative dispersion (RD) of a variable for varying scales of space or time
Relative dispersion	A measure of heterogeneity of a distribution (SD divided by mean of distribution)
Rescaled range analysis	Method of determining whether a structure or process is fractal and estimating the Hurst exponent. It is similar to RD analysis, in which the scale of measurement is a time period (τ) and the observed measurement is the local range divided by SD (R/SD) of observations. Hurst exponent is slope of log-log plot of τ vs. R/SD
Scale independence	A characteristic of fractal structures or processes where characteristic forms or fluctuations remain constant independent of the scale of measurement (self-similarity)
Self-similarity	A characteristic of fractal structures or processes where characteristic forms or fluctuations on a small scale of measurement are similar to those on a larger scale of measurement (scale independence)
Spatial correlation	A measure of the similarity in an observed variable between 2 adjacent regions. It can assume all real values between −1.0 and 1.0. A value of −1.0 indicates complete negative correlation, 0.0 represent a random relationship, and 1.0 indicates complete uniformity.

Temporal correlation	A measure of similarity in an observed variable between 2 adjacent observations in time. It can assume all real values between −1.0 and 1.0. A value of −1.0 indicates complete negative correlation, 0.0 represents a random relationship, and 1.0 indicates complete uniformity
Topological dimension	Smallest Euclidean dimension that an object can be reduced to by a 1:1 continuous point mapping (i.e., stretching but not tearing), e.g., a curved line can be reduced to a straight line of 1 dimension, and a curved surface can be reduced to a flat plane of 2 dimensions. It can assume only integer values. A branching line is topologically 1-dimensional but may require embedding in a plane or 3-dimensional space to reveal its form

Variables

β	Power spectrum exponent as measured by spectral analysis; $\beta = 0.0$ for white noise and $\beta = 2.0$ for Brownian motion
D_s	Spatial correlation as measured by RD analysis; $1.0 \le D_s \le 1.5$
D_τ	Temporal correlation as measured by RD analysis; $1.0 \le D_\tau \le 1.5$
E	Euclidean dimension
H	Hurst exponent
l	Measuring stick of a given length, l
l_0	Initial measuring stick length
$L(l)$	Apparent contour length of a structure using a measuring stick of length l
m	Mass of observed piece
m_0	Mass of reference piece, arbitrarily chosen
$N_{box}(l)$	Number of boxes of side length l covering the structure
R	Local range in Hurst analysis
RD_s	Relative dispersion of spatially oriented observations
RD_τ	Relative dispersion of temporally oriented observations
r_s	Spatial correlation between adjacent regions; $-1.0 \le r_s \le 1.0$.
r_τ	Temporal correlation between observations adjacent in time; $-1.0 \le r_\tau \le 1.0$
$r(n)$	Correlation between observations separated by n units of space or time
SD	Standard deviation of observations
v	Volume of observed region
v_0	Volume of reference region, arbitrarily chosen

Equations

$$\frac{L(l)}{L(l_0)} = \left(\frac{l}{l_0}\right)^{1-D}$$

$$\ln L(l) = (1-D)\ln\left(\frac{l}{l_0}\right) + \ln L(l)$$

$$\ln \mathrm{RD}_s(v) = (1-D_s)\ln\left(\frac{v}{v_0}\right) + \ln \mathrm{RD}_s(v_0)$$

$$\frac{\mathrm{RD}_s(v)}{\mathrm{RD}_s(v_0)}=\left(\frac{v}{v_0}\right)^{1-D_s}$$

$$\frac{\mathrm{RD}_s(m)}{\mathrm{RD}_s(m_0)}=\left(\frac{m}{m_0}\right)^{1-D_s}$$

$$r_s=2^{3-2D_s}-1$$

$$F=\gamma^k(1-\gamma)^{n-k}F_0$$

$$\frac{R/\mathrm{SD}\ \ \text{for}\ \ \text{interval}\,\tau}{R/\mathrm{SD}\ \ \text{for}\ \ \text{interval}\,\tau_0}=\left(\frac{\tau}{\tau_0}\right)^{H-1}$$

$$r(n)=\frac{\sum x_i(\tau)x_i(\tau+n\tau)}{\mathrm{Var}\,(x)}$$

$$r(n)={}^1/_2\left[|n+1|^{2H}-2n^{2H}+|n-1|^{2H}\right]$$

Appendix B

Figure 14 is an example of the RD method of fractal analysis for a time course signal. The demonstration data set is smaller than the recommended minimal size to facilitate working through the example with a hand calculator.

References

1. Bassingthwaighte JB. Physiological heterogeneity: fractals link determinism and randomness in structures and functions. News Physiol Sci. 1988; 3:5–10. [PubMed: 20871797]
2. Bassingthwaighte JB, King RB, Roger SA. Fractal nature of regional myocardial blood flow heterogeneity. Circ Res. 1989; 65:578–590. [PubMed: 2766485]
3. Bassingthwaighte JB, van Beek JHGM. Lightning and the heart: fractal behavior in cardiac function. Proc IEEE. 1988; 76:693–699.
4. Feder, J. Fractals. New York: Plenum; 1988.
5. Glenny RW, Robertson HT. Fractal properties of pulmonary blood flow: characterization of spatial heterogeneity. J Appl Physiol. 1990; 69:532–545. [PubMed: 2228863]
6. Glenny RW, Robertson HT. Fractal modeling of pulmonary blood flow heterogeneity. J Appl Physiol. 1991; 70:1024–1030. [PubMed: 2032967]

7. Goldberger AL, Bhargava, West BJ, Mandell AJ. On a mechanism of cardiac electrical stability. The fractal hypothesis. Biophys J. 1985; 48:525–528. [PubMed: 4041542]
8. Goldberger AL, Rigney DR, West BJ. Chaos and fractals in human physiology. Sci Am. 1990; 262:42–49. [PubMed: 2296715]
9. Horsfield K. Morphometry of the small pulmonary arteries in man. Circ Res. 1978; 42:593–597. [PubMed: 639181]
10. Horsfield K. Diameters, generations, and orders of branches in the bronchial tree. J Appl Physiol. 1990; 68:457–461. [PubMed: 2318756]
11. Horsfield K, Cumming G. Morphology of the bronchial tree in man. J Appl Physiol. 1968; 24:373–383. [PubMed: 5640724]
12. Horsfield K, Relea FG, Cumming G. Diameter, length, and branching ratios on the bronchial tree. Respir Physiol. 1976; 26:351–356. [PubMed: 951538]
13. Horsfield K, Woldenberg MJ. Diameters and cross-sectional areas of branches in the human pulmonary arterial tree. Anat Rec. 1989; 223:245–251. [PubMed: 2923275]
14. Hurst, HE.; Black, RP.; Simaiki, YM. Long-Term Storage: An Experimental Study. London: Constable; 1965.
15. Kislyakov YY, Levkovitch YI, Shuymilova TE, Vershinina EA. Blood flow fluctuations in cerebral cortex microvessels. Int J Microcirc Clin Exp. 1987; 6:3–13. [PubMed: 3583576]
16. Kuhn, TS. International Encyclopedia of Unified Science. Chicago: University of Chicago Press; 1970. The structure of scientific revolutions.
17. Langman, J. Medical Embryology. Human Development—Normal and Abnormal. 3rd. Baltimore, MD: Williams & Wilkins; 1975.
18. Lefèvre J. Teleonomical optimization of a fractal model of the pulmonary arterial bed. J Theor Biol. 1983; 102:225–248. [PubMed: 6876845]
19. Lewis M, Rees DC. Fractal surfaces of proteins. Science Wash DC. 1985; 230:1163–1165.
20. Liebovitch LS, Fischbarg J, Koniarek JP, Todorova I, Wang M. Fractal model of ion-channel kinetics. Biochim Biophys Acta. 1987; 896:173–180. [PubMed: 2432935]
20a. Liebovitch LS, Toth TI. A fast algorithm to determine fractal dimensions by box counting. Phys Lett A. 1989; 141:386–390.
21. Lovejoy S, Mandelbrot BB. Fractal properties of rain, and a fractal model. Tellus. 1985; 37A:209–232.
22. MacDonald, N. Trees and Networks in Biological Models. New York: Wiley; 1983.
23. Mandelbrot BB. How long is the coast of Britain? Statistical self-similarity and fractional dimension. Science Wash DC. 1967; 156:636–638.
24. Mandelbrot, BB. The Fractal Geometry of Nature. San Francisco: Freeman; 1983.
25. Mandelbrot BB, Wallis JR. Some long-run properties of geophysical records. Water Resour Res. 1969; 5:321–340.
26. Massoud EAS, Rotschild A, Matsui R, Sekhon HS, Thurlbeck WM. In vitro airway branching morphogenesis of the fetal rat lung. (Abstract). Am Rev Respir Dis. 1990; 141:A340.
27. Meakin P. A new model for biological pattern formation. J Theor Biol. 1986; 118:101–113. [PubMed: 3702470]
28. Nelson, TR. Medical Imaging II: Image Formation Detection, Processing, and Interpretation/Image Data Management and Display. Bellingham, WA: SPIE-Int Soc Opt Eng; 1988. Morphological modeling using fractal geometries; p. 326-333.
29. Nelson TR, Manchester DK. Modeling of lung morphogenesis using fractal geometries. IEEE Trans Med Imaging. 1988; 7:321–327. [PubMed: 18230485]
30. Oude Vrielink HHE, Slaaf DW, Tangelder GJ, Weijmer-Van Velzen S, Reneman RS. Analysis of vasomotion waveform changes during pressure reduction and adenosine application. Am J Physiol. 1990; 258(Heart Circ. Physiol. 27):H29–H37. [PubMed: 2301612]
31. Raabe, OG.; Yeh, HC.; Schum, GM.; Phalen, RF. Tracheobronchial Geometry: Human, Dog, Rat, Hamster. Washington DC: US Govt. Printing Office; 1976.
32. Rigaut JP. An empirical formulation relating boundary lengths to resolution in specimens showing non-ideally fractal dimensions. J Microsc. 1984; 133:41–54.

33. Sander LM. Fractal growth. Sci Am. 1987; 256:94–100.
34. Singhal S, Henderson R, Horsfield K, Harding K, Cumming G. Morphometry of the human pulmonary arterial tree. Circ Res. 1973; 33:190–197. [PubMed: 4727370]
35. Smith TG Jr, Marks WB, Lange GD, Sheriff WH Jr, Neale EA. A fractal analysis of cell images. J Neurosci Methods. 1989; 27:173–180. [PubMed: 2709885]
36. Tsonis AA, Tsonis PA. Fractals: a new look at biological shape and patterning. Perspect Biol Med. 1987; 30:355–361. [PubMed: 3588239]
37. Van Beek JHGM, Roger SA, Bassingthwaighte JB. Regional myocardial flow heterogeneity explained with fractal networks. Am J Physiol. 1989; 257(Heart Circ. Physiol. 26):H1670–H1680. [PubMed: 2589520]
38. Van Roy, P.; Garcia, L.; Wahl, B. Designer Fractal. Mathematics for the 21st Century. Santa Cruz, CA: Dynamic Software; 1988.
39. Voss, RF. Fractals in nature: from characterization to simulation. In: Peitgen, HO.; Saupe, D., editors. The Science of Fractal Images. New York: Springer-Verlag; 1988. p. 21-70.
40. Voss RF, Clark J. “1/f Noise” in music and speech. Nature Lond. 1975; 258:317–318.
41. Weibel ER, Gomez DM. Architecture of the human lung. Science Wash DC. 1962; 137:577–585.
42. West BJ, Bhargava V, Goldberger AL. Beyond the principle of similitude: renormalization in the bronchial tree. J Appl Physiol. 1986; 60:1089–1097. [PubMed: 3957825]
43. West BJ, Goldberger AL. Physiology in fractal dimensions. Am Sci. 1987; 75:354–365.
44. Bassingthwaighte JB, Beyer RP. Fractal correlation in heterogeneous systems. Physica D. 1991; 53:71–84.

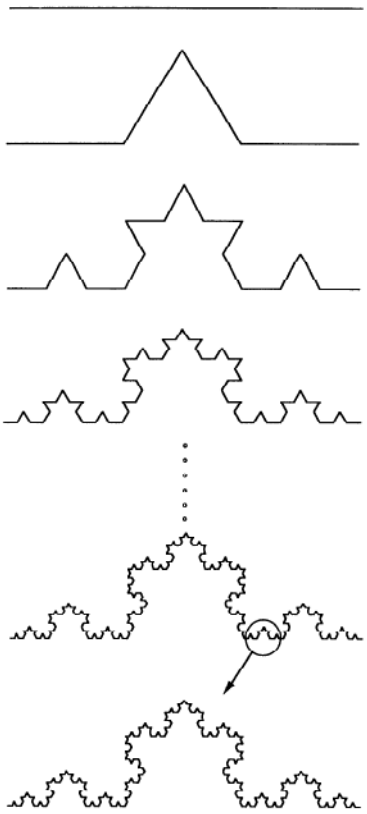

FIG. 1.

Generation of Koch curve produced by a simple iterative transformation beginning with a straight line (*top*). At each step, middle third of each line segment is replaced with 2 segments, one-third of the length of the line, forming part of an equilateral triangle. Completed curve has an infinite number of iterations. Regardless of magnification of scale, any part of the curve resembles the whole (*bottom*). [From Glenny and Robertson (5).]

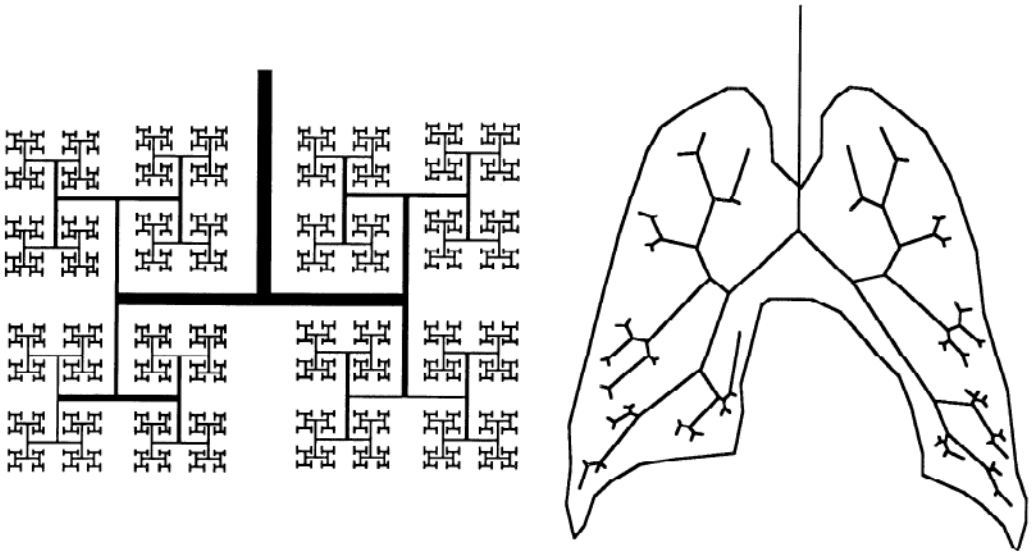

FIG. 2.

Two-dimensional representations of bronchial tree. *Left*: symmetrical bifurcating network with 90° branching angles and length segments scaled proportionally from parent branch (similar to Mandelbrot's model of the lung). *Right*: more realistic model in which branching segments fill a predetermined boundary. [From Nelson and Manchester (29).]

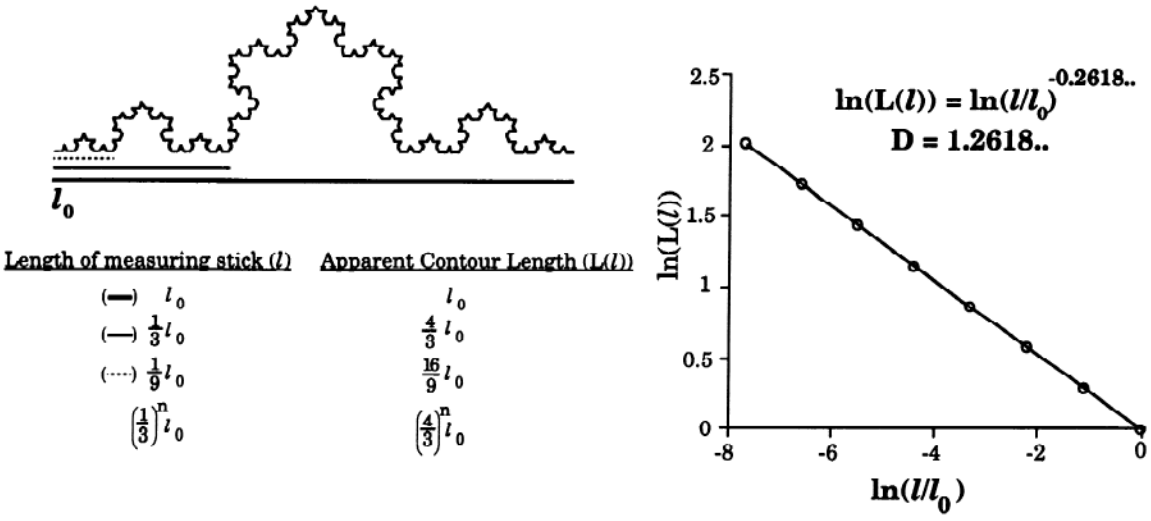

FIG. 3.

Apparent contour length of Koch curve is dependent on length of measuring stick. *Left*: the finer the scale (greater magnification), the greater the apparent length of the curve. *Right*: fractal (log-log) plot of apparent length, $L(l)$, of Koch curve as a function length of measuring device, l relative to l_0. Line through points represents least-squares linear regression fit. Relationship appears linear with a slope of −0.2618 … and thus a fractal dimension (D) of 1.2618. …

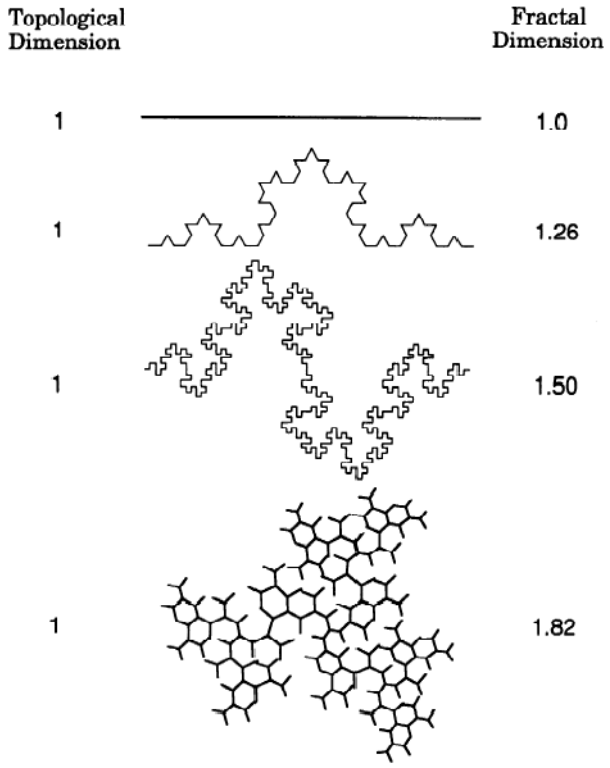

FIG. 4.

Lines of topological *dimension 1* with different fractal dimensions. Fractal dimension is bounded by topological dimension and Euclidean dimension (in this case, *dimensions 1* and *2*). The greater the irregularity of the line, or the more space it fills, the greater the fractal dimension. [From Glenny and Robertson (5).]

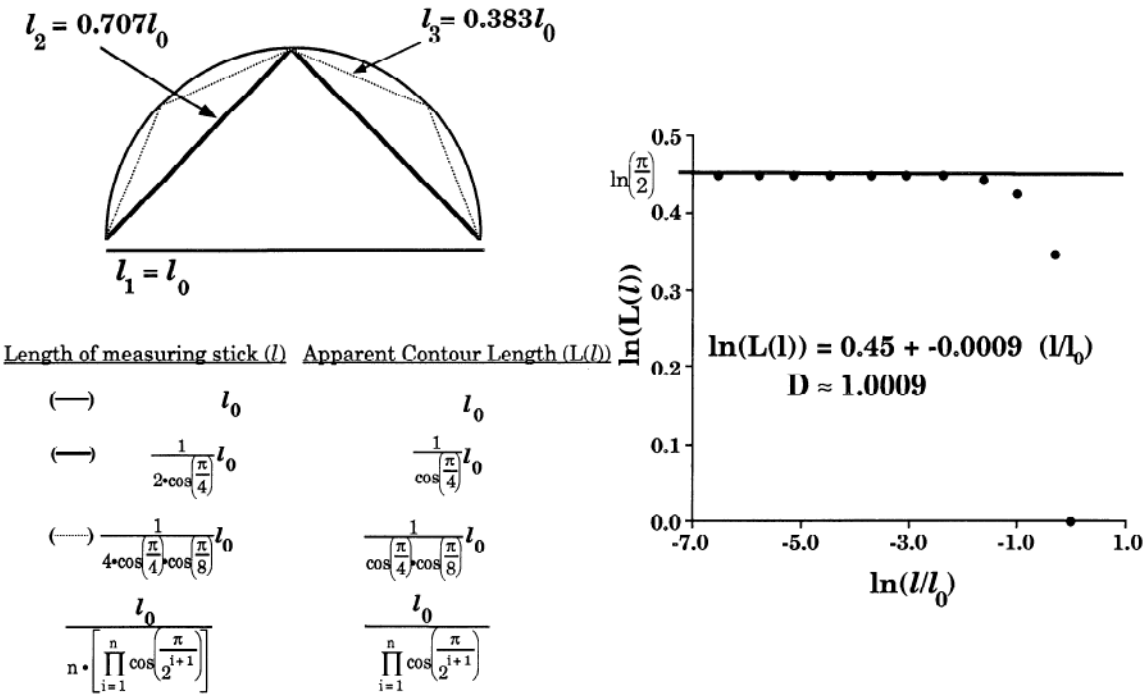

FIG. 5.

Fractal analysis of a semicircle, which is not fractal. *Left*: apparent contour length of curve is initially determined by a measuring stick of length l_0 equal to diameter of semicircle. Measuring stick is then repeatedly shortened so that at each iteration (n) it bisects distance around curve between prior cords. Apparent length of curve, $L(l)$, at each iteration can be determined, and as n increases, $L(l)$ goes to $\pi l_0/2$. *Right*: fractal plot of $L(l)$ as a function of length of measuring stick, l relative to l_0. Line represents weighted least-squares fit to data; slope of this line is −0.0009.

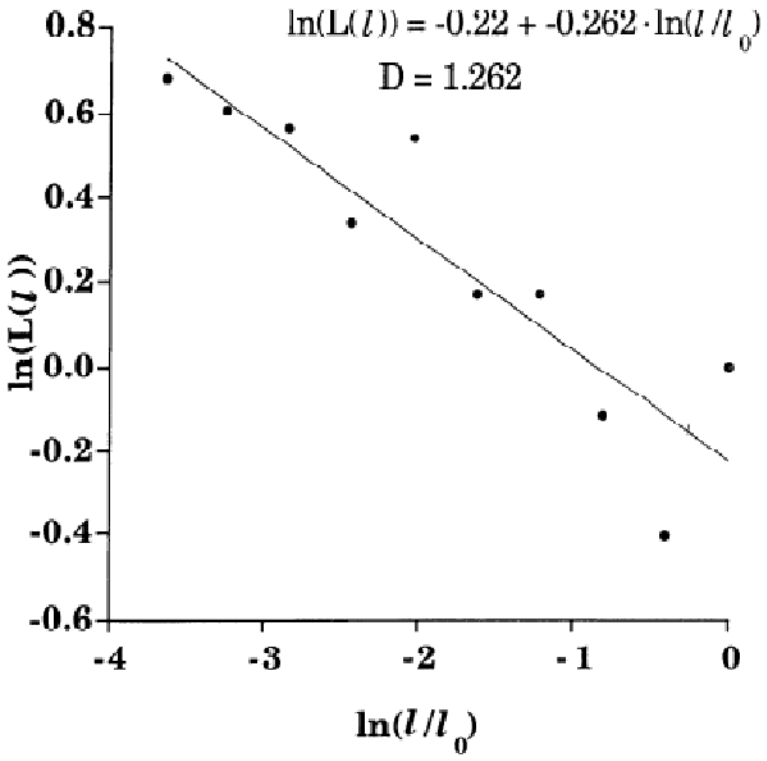

FIG. 6.

Apparent contour length of Koch curve where measuring stick, *l*, is two-thirds the length of previous measuring stick. Linear fit to log-log data of apparent contour length *L*(*l*) as a function of measuring stick length is not as good as in Fig. 3 (*right*), where a different measuring stick length was used.

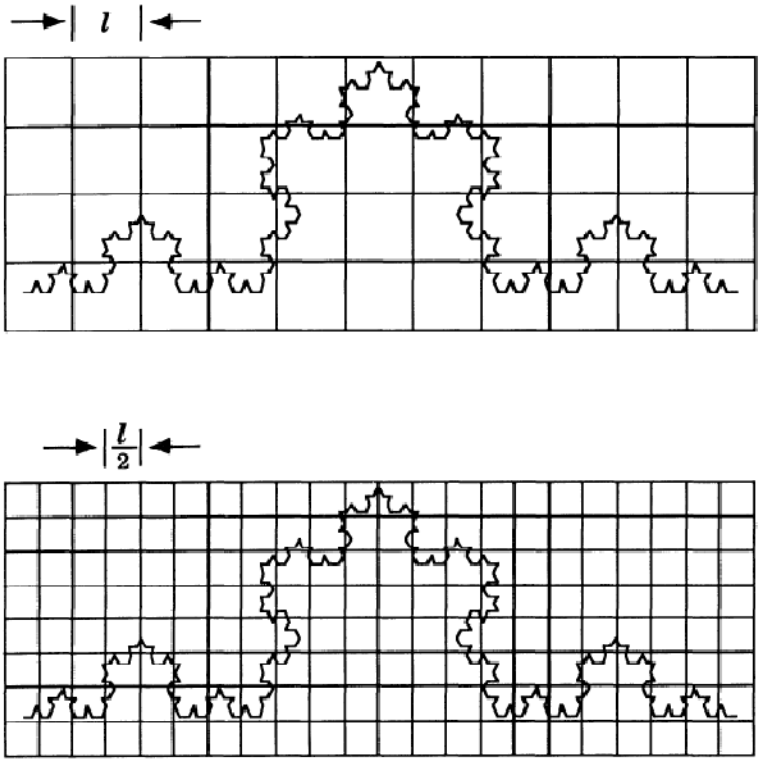

FIG. 7.

Box or grid approach to determining fractal dimension of an object. Number of boxes containing a portion of curve, $N_{box}(l)$, is determined for progressively smaller box dimensions, *l*. *Top*: $N_{box}(l) = 23$ of the 44 boxes. *Bottom*: when *l* is decreased by one-half, $N_{box}(l/2) = 56$ of the 176 boxes. Fractal dimension can be determined from log-log plot of $N_{box}(l)$ as a function of *l*.

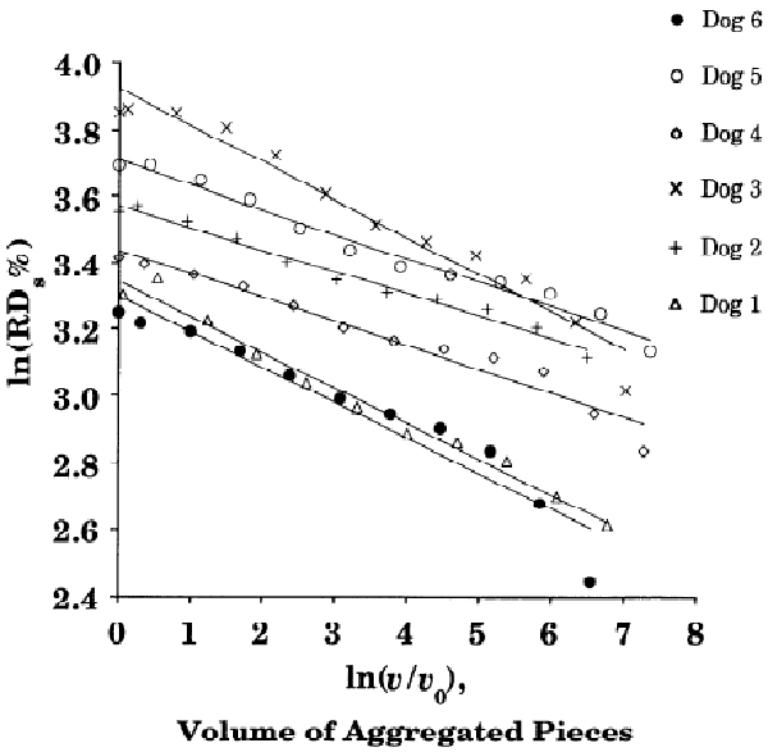

FIG. 8.

Relative dispersion (RD) of regional pulmonary blood flows plotted as a function of volume of aggregated lung pieces. Smallest regions (v_0) are “voxels” from a planar gamma camera in which voxels are 1.5 × 1.5 × 11.5 mm or 24 mm^3. [From Glenny and Robertson (5).]

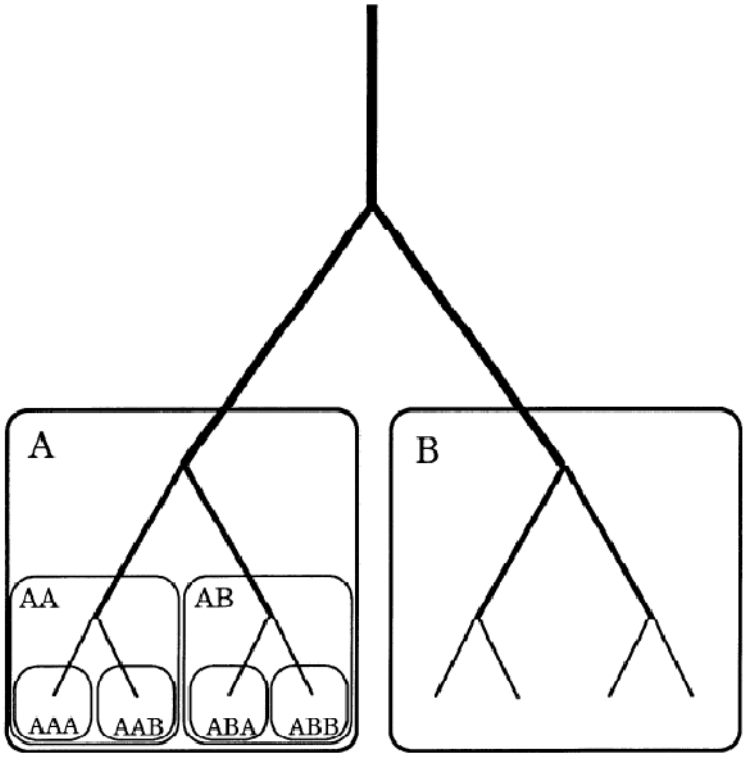

FIG. 9.

Schematic representation of regional vascular perfusion to an organ. If blood flow distribution is fractal, then blood flow in adjacent pieces will have the same correlation regardless of size.

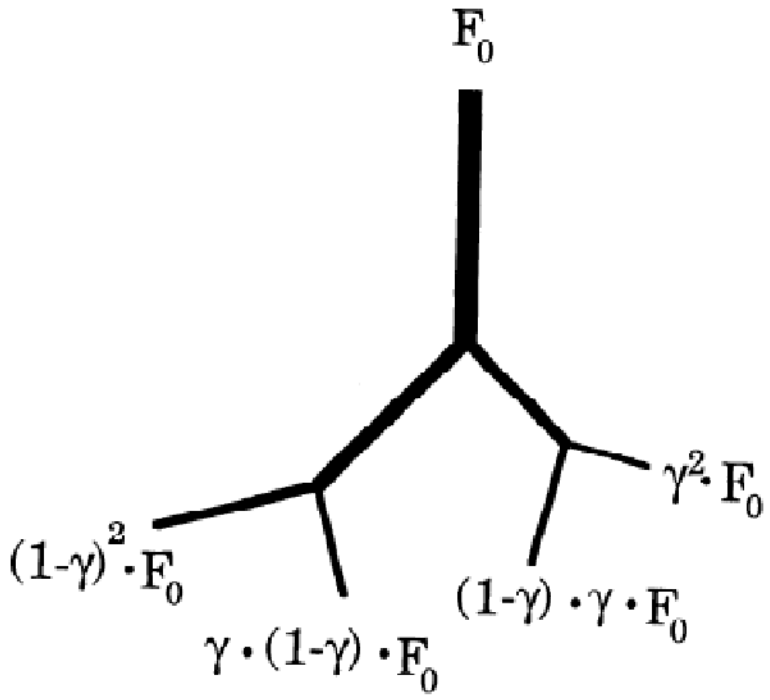

FIG. 10.

Asymmetric fractal branching network in which relative fraction of blood flow from parent segment to daughter branches is γ and $1 - \gamma$. Flow at each segment of network can be determined given flow into network (F_0), and RD of blood flow can be calculated as a function of γ.

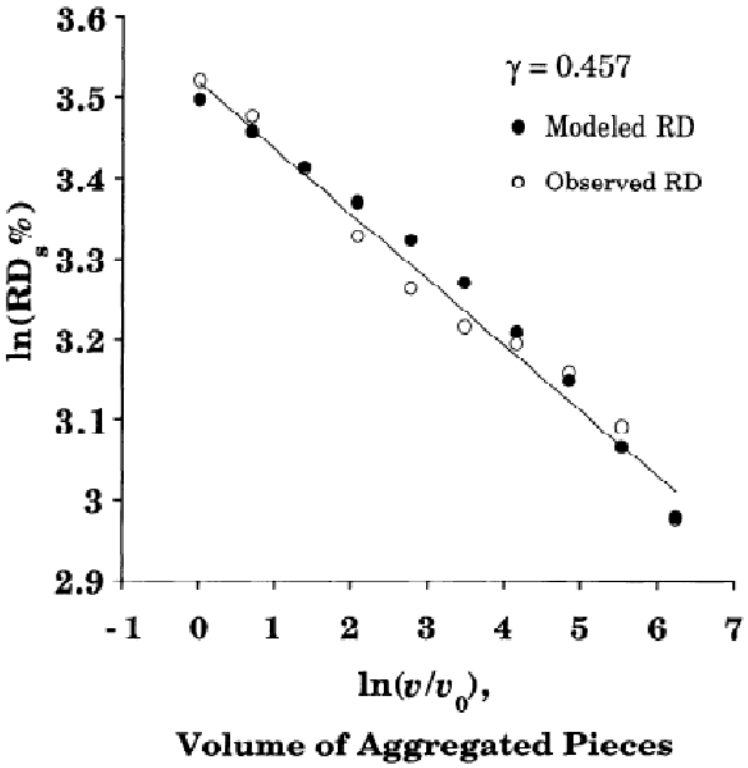

FIG. 11.

Optimized fit of modeled data to actual RD data from a dog lung. Best fit of branching network model to data yields a γ of 0.457. Note slight downward concavity of dichotomously branching network model (v_0 = voxel size = 24 mm^3).

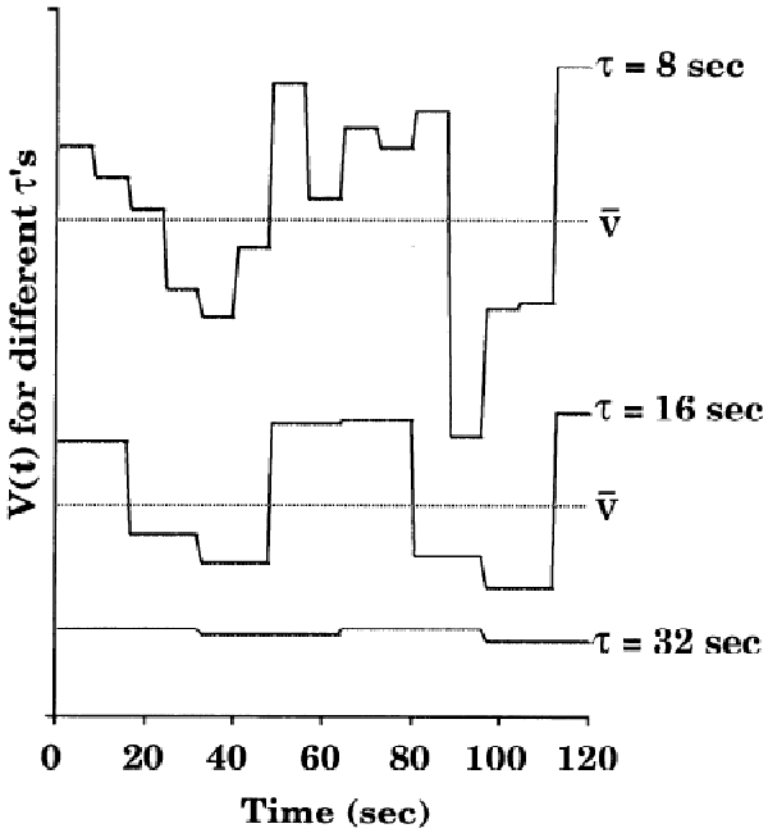

FIG. 12.

Top curve: V(*t*) as a function of time at uniform intervals, $\tau = 8$ s. *Bottom 2 curves*: successive averages over intervals (τ) of double the length. Note diminution in dispersion with successive lumpings.

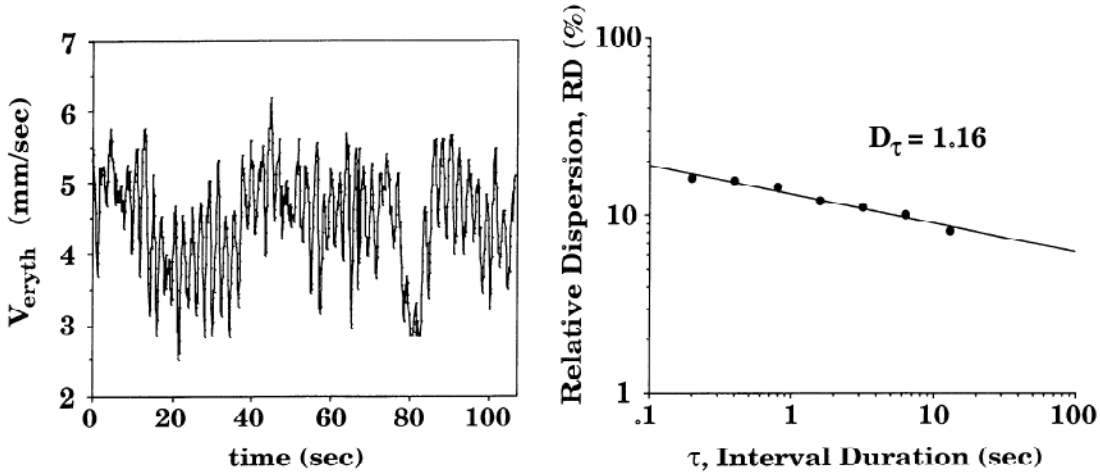

FIG. 13.

Fractal (RD) analysis of vasomotion. *Left*: erythrocyte velocities (V_{eryth}) in a 7-μm arteriole of rabbit tenussimus muscle with Δt = 0.1 s. [Data from Oude Vrielink et al. (30).] *Right*: RD of velocities averaged over intervals of length τ decreases with increasing τ and has an apparent D of 1.162.

t	V(t)					
1	10.31					
2	19.03	14.67				
3	34.7					
4	19.26	26.98	20.83			
5	65.42					
6	34.79	50.11				
7	19.07					
8	35.34	27.21	38.66	29.74		
9	34.82					
10	18.80	26.81				
11	18.69					
12	10.28	14.49	20.65			
13	10.03					
14	10.12	14.58				
15	5.58					
16	10.07	7.83	11.20	15.92	22.83	
17	35.52					
18	19.28	27.4				
19	35.38					
20	64.40	50.14	38.77			
21	66.83					
22	35.61	51.22				
23	121.34					
24	64.34	92.84	72.03	55.4		
25	19.35					
26	35.78	27.57				
27	35.77					
28	64.38	50.08	38.82			
29	10.04					
30	19.10	14.57				
31	18.82					
32	35.52	27.17	20.87	29.85	42.62	32.73
33	35.36					
34	19.28	27.32				
35	19.00					
36	10.06	14.53	20.93			
37	35.78					
38	18.94	27.36				
39	66.09					
40	34.90	50.50	38.93	29.93		
41	64.76					
42	34.91	49.84				
43	35.16					
44	18.89	27.03	38.43			
45	54.39					
46	35.09	49.74				
47	66.18					
48	121.58	93.86	71.81	55.12	42.52	
49	122.48					
50	229.45	175.97				
51	120.93					
52	66.25	93.59	134.78			
53	66.75					
54	34.95	50.85				
55	119.86					
56	64.75	92.31	71.58	103.18		
57	121.15					
58	65.03	93.09				
59	64.8					
60	36.00	50.4	71.75			
61	64.91					
62	35.59	50.25				
63	19.33					
64	35.71	27.52	38.89	55.32	79.25	50.88
Mean	46.81	46.81	46.81	46.81	46.81	46.81
SD	38.97	35.05	31.19	27.28	23.54	19.91
RD%	83.25	74.88	66.63	58.26	50.29	42.53
ln(RD%)	4.42	4.32	4.20	4.07	3.92	3.75
N	64	32	16	8	4	2
Size (τ)	1	2	4	8	16	32
ln(τ)	0	0.69	1.39	2.08	2.77	3.47

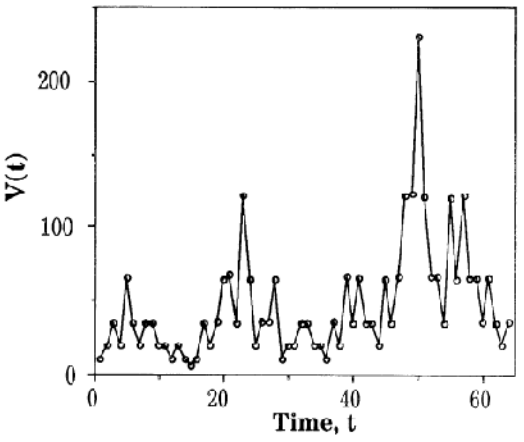

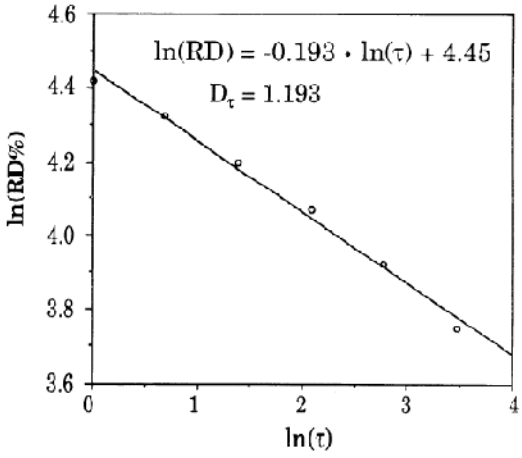

FIG. 14.

RD method of fractal analysis for a time course signal. Columns *t* (in arbitrary units) and V(*t*) (value of signal at *time t*) represent original time course signal sampled at given temporal resolution. *Top right*: 64 observations presented in graphical form. *Bottom right*: mean, SD, RD (RD% = 100 · SD/mean), and other necessary calculations. Column to the right of V(*t*) is obtained by averaging 2 adjacent measurements of original data to make 1 observation. *N* has now been reduced to 32, and time interval has increased to 2. Mean, SD, and RD are again calculated for a new grouping of data with RD = 74.88%. If scale of time

interval is increased again by averaging every 2 points of the new data set ($\tau = 4$), a new RD can be calculated. This process is continued until there are only 2 data points and $\tau = 32$, which results in 6 measurements of RD at 6 different scales of resolution. D_τ is obtained by plotting logarithm of RD against logarithm of time interval (τ). At *bottom right*, a least-squares linear fit to data and slope of line used to calculate fractal dimension (slope = $1 - D_\tau$) are obtained. Fractal dimension of observations presented is 1.19 and, as expected, $1.0 \leq D_\tau \leq 1.5$.

TABLE 1

Spatial heterogeneity of cardiac blood flow and fractal dimensions for pulmonary blood flow

	No. of Animals	D_s	Mean r_s
Baboon hearts	10	1.21+0.04	0.49
Sheep hearts	11	1.17±0.06	0.58
Rabbit hearts	6	1.25±0.07	0.41
Dog lungs	6	1.09±0.02	0.76